

SCIENTIFIC REPORTS

OPEN

Robust numerical evaluation of circular dichroism from chiral medium/nanostructure coupled systems using the finite-element method

Seoo Lee¹, Ji-Hun Kang¹, SeokJae Yoo¹ & Q-Han Park¹

It has been demonstrated that circular dichroism (CD) signals from chiral molecules can be boosted by plasmonic nanostructures inducing strong local electromagnetic fields. To optimize nanostructures to improve CD enhancement, numerical simulations such as the finite element method (FEM) have been widely adopted. However, FEM calculations for CD have been frequently hampered by unwanted numerical artifacts due to improperly discretizing problem spaces. Here, we introduce a new meshing rule for FEM that provides CD simulations with superior numerical accuracy. We show that unwanted numerical artifacts can be suppressed by implementing the mirror-symmetric mesh configuration that generates identical numerical artifacts in the two-opposite circularly polarized waves, which cancel each other out in the final CD result. By applying our meshing scheme, we demonstrate a nanostructure/chiral molecule coupled system from which the CD signal is significantly enhanced. Since our meshing scheme addresses the previously unresolved issue of discriminating between very small CD signals and numerical errors, it can be directly applied to numerical simulations featuring natural chiral molecules which have intrinsically weak chiroptical responses.

Circular dichroism (CD) can be found in various natural substances including molecules and crystals and is of particular importance to the study of biology and chemistry^{1,2}. Because the interaction of incident light with chiral molecules is generally quite weak, nanostructure-molecule coupling has been proposed as a way to enhance CD by inducing strong near fields that boost the optical helicity density of the incident light^{3–17}. Various numerical schemes^{18–20} including the finite element method (FEM)^{12,21–23} have been widely adopted to estimate enhancements in optical helicity density and optimize the nanostructures. However, for CD calculations, FEM has been used without in-depth consideration of meshing, i.e., the discretization of the problem space, so possible numerical artifacts arising from meshing have not been taken into account. Since CD calculation demands a difference between two signals, the left- and right-circularly polarized lights, numerical artifacts can be cumulative when not consistently generated by the two different polarizations.

In this paper, we introduce a new meshing scheme, mirror symmetric mesh (MSM), that possesses a mirror symmetry with the mirror plane containing the light wavevector. Such a MSM provide a symmetric mesh configuration against the left- and right-circularly polarized lights. MSM can be applied to FEM for CD calculations which features suppressed numerical artifacts. Non-negligible numerical artifacts arise especially when the chiral medium is coupled with nanostructures, and they become noticeably stronger when the implementation of a periodic structure is required. We show that, compared to the usual non-mirror symmetric mesh (non-MSM) shown in Fig. 1(a), our MSM scheme shown in Fig. 1(b) provides superior numerical accuracy by eliminating the unwanted numerical artifacts in such a way that they cancel each other out in the final CD calculations. Our meshing scheme was tested on the calculation of the CD of a chiral molecule/nanodisk coupled system, and we

¹Department of Physics, Korea University, Seoul, 02841, Korea. ²Department of Physics and Astronomy, Seoul National University, Seoul, 08826, Korea. Correspondence and requests for materials should be addressed to Q.-H.P. (email: qpark@korea.ac.kr)

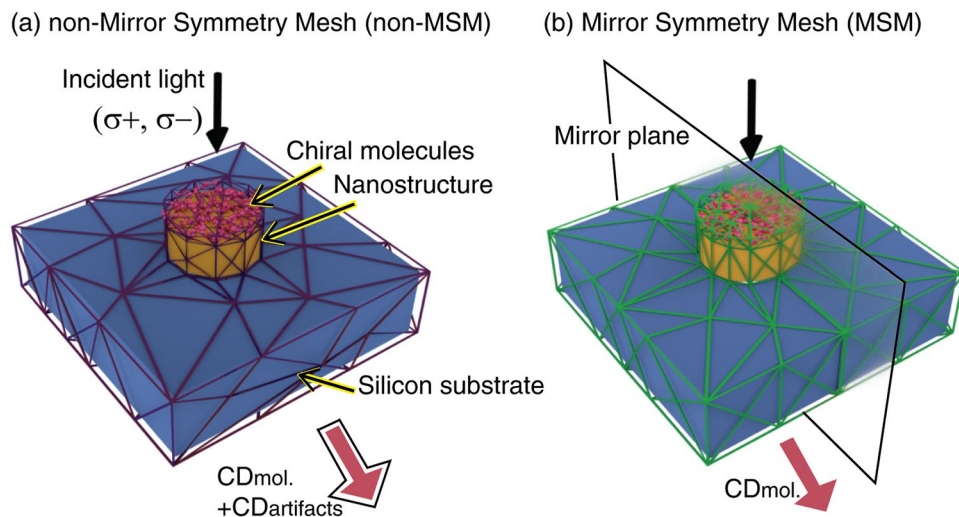


Figure 1. Schematics of non-mirror symmetric mesh (non-MSM) and mirror symmetric mesh (MSM). Discretized chiral molecule/gold nanostructure coupled system by (a) non-MSM and (b) MSM. MSM has a mirror symmetry with respect to the mirror plane.

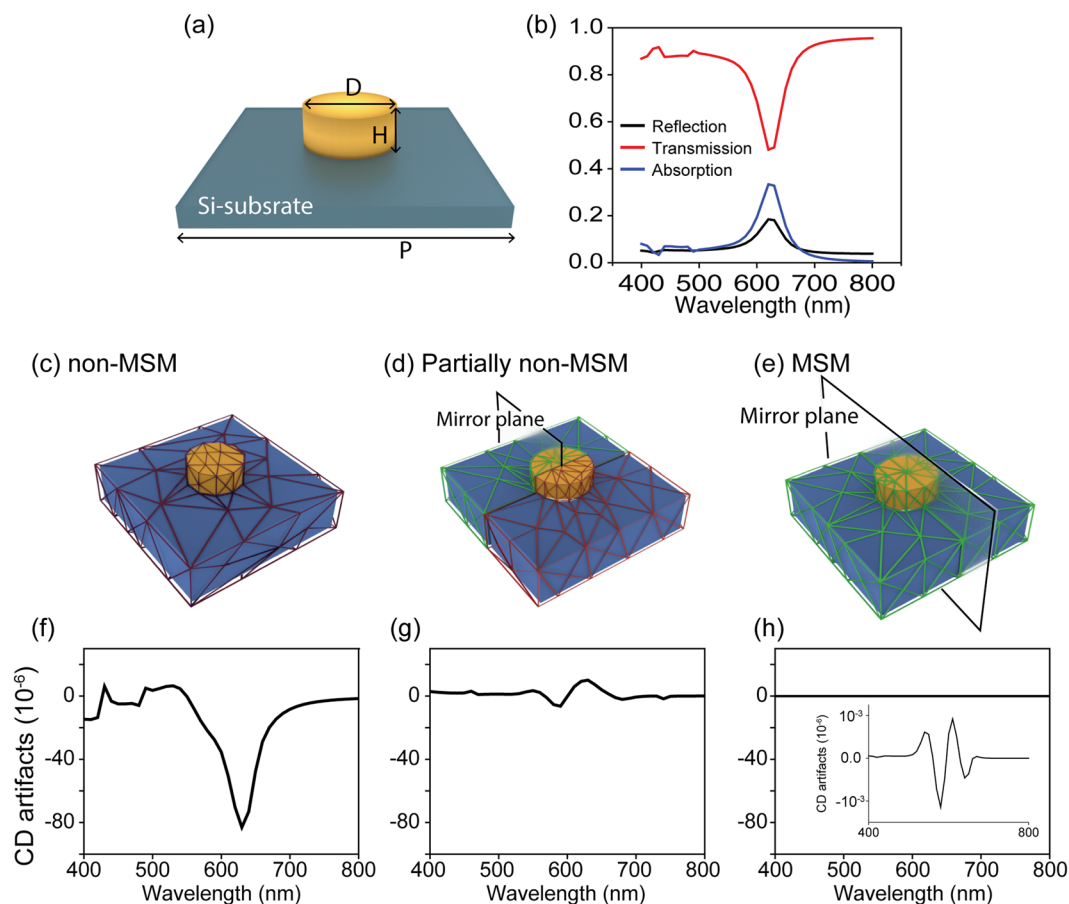


Figure 2. Impact of the discrete meshes on calculations of the optical responses of the gold nanodisk. (a) A schematic of a gold nanostructure of diameter $D = 90$ nm, height $H = 30$ nm, and lattice constant $L = 350$ nm. (b) Reflection, transmission, and absorption spectra of the gold nanodisk with circularly polarized incident light. Schematics of the discretization of the problem space using (c) non-MSM, (d) partially non-MSM, and (e) MSM schemes and their corresponding numerical artifacts, CD_{mesh} , in (f–h), respectively.

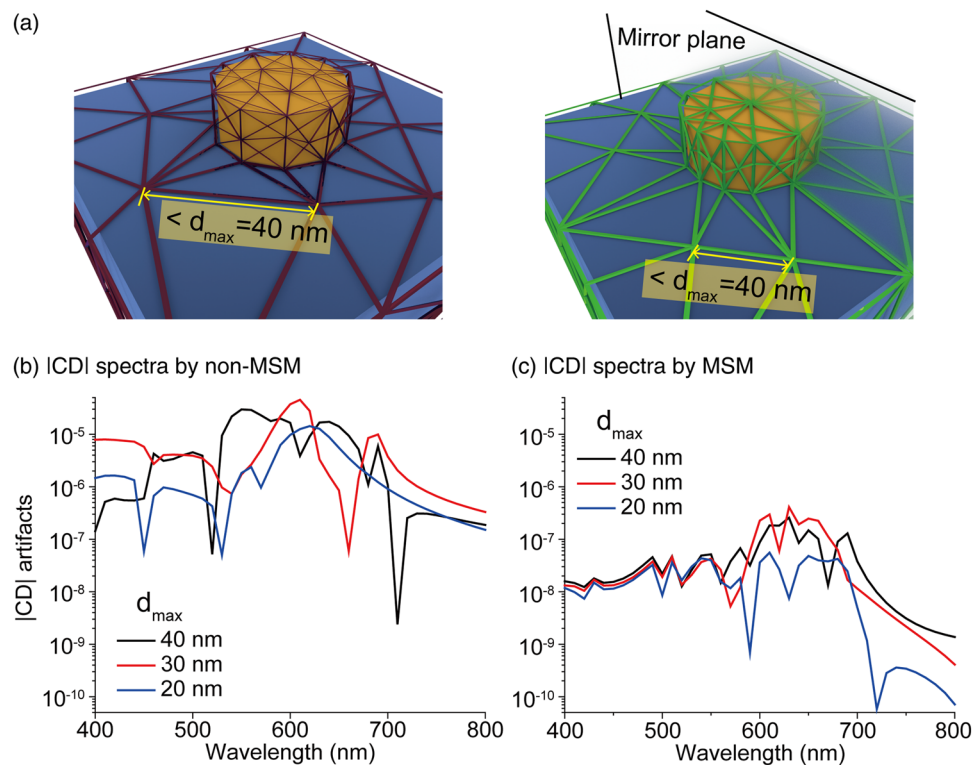


Figure 3. Convergence test of CD_{mesh} from non-MSM and MSM with three different maximum grid sizes. (a) Schematics of non-MSM and MSM. We set three maximum grid size (d_{max}) as 40 nm, 30 nm and 20 nm. The CD_{mesh} spectra from (b) non-MSM and (c) MSM are present.

show that our scheme exhibits much faster numerical convergence regarding finite-element grid size than the usual meshing schemes, which require much finer grids and longer computation times to achieve convergence.

Results

Numerical CD artifacts from broken mirror-symmetric mesh. Because the CD signals of chiral molecules are usually very weak^{24–26}, in their case eliminating the numerical artifacts caused by mesh (CD_{mesh}) is particularly important. Here, we start by demonstrating how CD_{mesh} can arise, by considering the achiral nanostructure shown in Fig. 2(a) and show the calculated artifact CD that should not exist in the system. The simulated reflection, transmission, and absorption spectra of the gold nanodisk show localized surface plasmon resonance (LSPR) at the wavelength of 620 nm. Note that, since the system is achiral, the spectra in Fig. 2(b) are independent of the polarization of the circularly-polarized incidence. Now, we calculate the CD signals for the three meshing configurations: the non-mirror symmetric mesh (non-MSM) (Fig. 2(c)), the partially non-MSM (Fig. 2(d)), and the mirror symmetric mesh (MSM) (Fig. 2(e)). The non-MSM lacks mirror symmetry, while the MSM possesses mirror symmetric geometry with respect to the mirror plane. The partially non-MSM, included to demonstrate how the meshing configuration impacts the CD_{mesh} , has mirror symmetry in only half of the system. For all three configurations, we set the maximum element size of the mesh (d_{max}) as 40 nm. As shown in Fig. 2(f,g), although in the achiral nanostructure there should be no CD signal⁷, the non-MSM and partially non-MSM configurations produce non-zero CD signals that are actually pure numerical artifacts from the mesh, CD_{mesh} . We note that those CD_{mesh} are maximized at the LSPR wavelength. We also point out that CD_{mesh} from the partially non-MSM is significantly suppressed compared to that from the non-MSM. This is significant because it implies that CD_{mesh} is a numerical artifact arising from an improperly discretized problem space, and that it can be suppressed by employing the MSM configuration. As shown in Fig. 2(h), the MSM perfectly eliminates the CD_{mesh} which agrees with the expected optical response of an achiral nanostructure. The MSM almost eliminates the CD_{mesh} because it produces the same amounts of numerical artifacts from the left circular polarized (LCP) and right circular polarized (RCP) waves and so they eventually cancel each other out during the calculation of the CD, which is the difference between the LCP and RCP signals.

In order to see the grid-size-dependency of CD_{mesh} with non-MSM and MSM, we calculated the CD_{mesh} from the achiral nanostructure implemented with three different maximum grid sizes, $d_{gold} = 40$ nm, 30 nm, and 20 nm, as shown in Fig. 3(a). The spectra of CD_{mesh} from non-MSM and MSM are present in Fig. 3(b,c), respectively. We found that overall CD_{mesh} from the non-MSM and the MSM all become reduced in a convergent way as the maximum mesh size decreases. However, even the converging CD_{mesh} arising from the non-MSM is much larger than the MSM. These results confirm that, compared to non-MSM, the suppression of CD_{mesh} by MSM is quite strong even with sparse meshes, allowing much more efficient numerical calculation of CD.

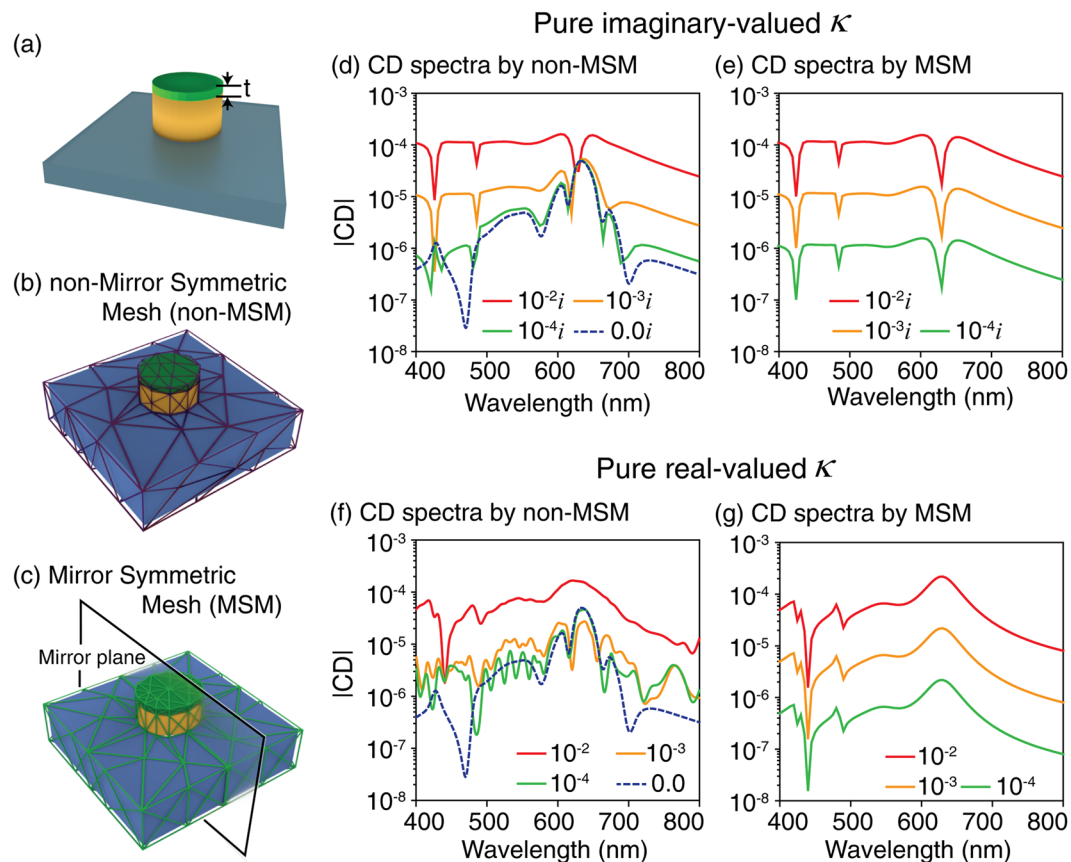


Figure 4. CD spectra from the chiral molecule/nanostructure coupled system with various values of chiral parameter κ . (a–c) Schematics of the coupled system, non-MSM and MSM. FEM-calculated CD spectra with purely imaginary-valued κ obtained using (d) MSM and (e) non-MSM. CD spectra with pure-real κ using (f) MSM and (g) non-MSM. The dotted blue curve in (d) is a CD spectrum with $\kappa = 0$, corresponding to CD_{mesh} . In the calculations, the thickness of the chiral medium, t , is set at 5 nm.

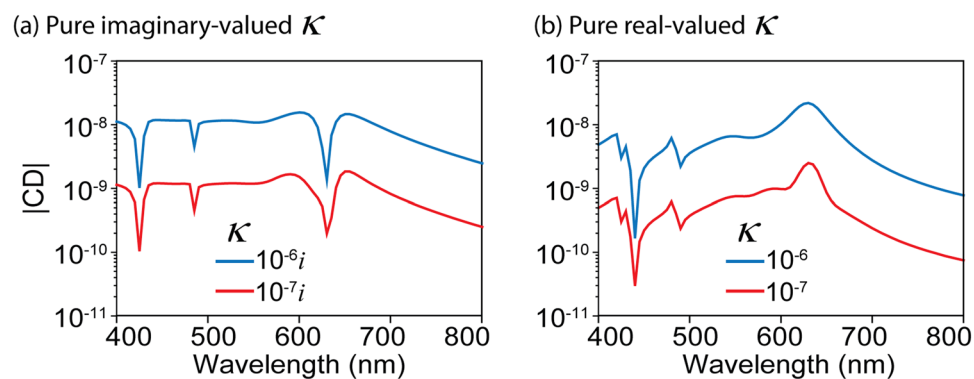


Figure 5. CD spectra with extremely small κ calculated by applying MSM. CD spectra with (a) pure-imaginary and (b) pure real κ .

CD spectra of the chiral molecule/nanostructure coupled system using non-MSM and MSM. Now, we apply our meshing scheme to the calculation of CDs by considering chiral media. As shown in Fig. 4(a), the chiral molecule which is considered as a homogenous medium of thickness $t = 5$ nm is coated onto the same nanostructure used in Fig. 2. The chiral media, which are different from the achiral media that can be considered as linear media, can be implemented by considering their constitutive relations defined as^{1,2}:

$$\mathbf{D} = \varepsilon\varepsilon_0\mathbf{E} + i\kappa\mathbf{H}/c_0, \quad (1)$$

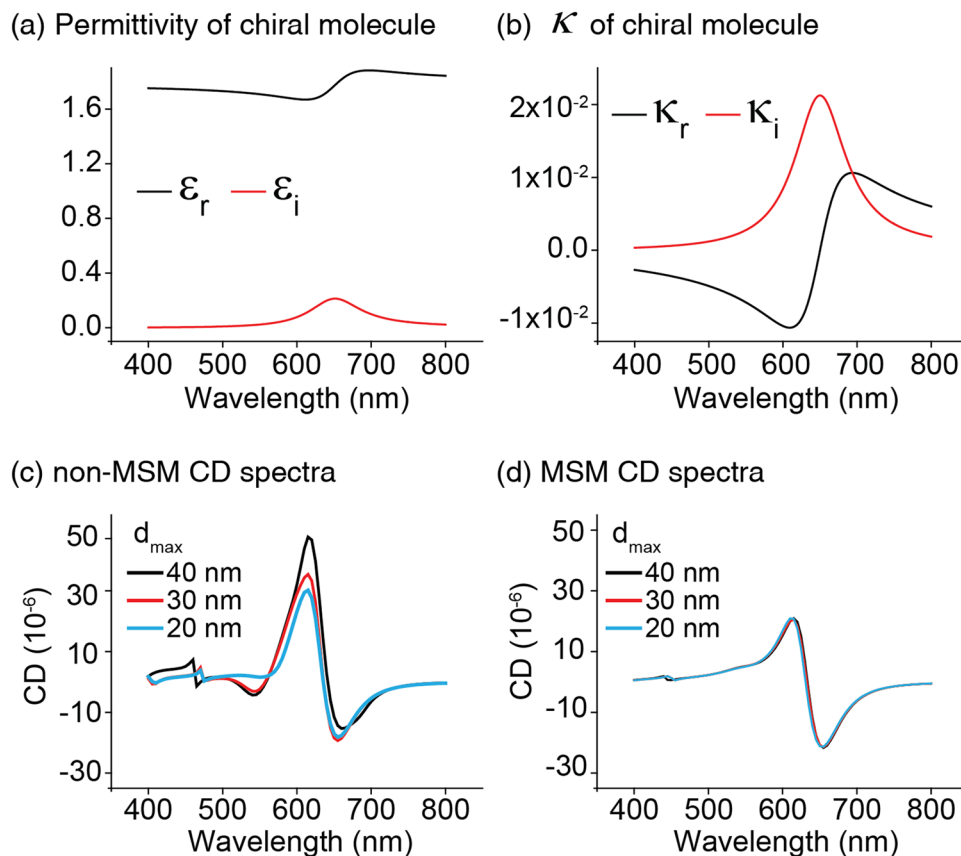


Figure 6. Numerical convergence test of CD spectra with decreasing maximum finite element size. **(a,b)** Assumed frequency dependence of the dielectric constant and chiral parameter κ of the chiral molecules. CD spectra obtained by **(c)** non-MSM and **(d)** MSM with various maximum grid sizes. In **(d)**, MSM gives almost identical CD spectra regardless of the maximum grid size, while in **(c)** non-MSM yields spectra that are not fully saturated. In the calculations, we set $t = 3$ nm.

$$\mathbf{B} = \mu\mu_0\mathbf{H} - i\kappa\mathbf{E}/c_0. \quad (2)$$

Here, ε_0 and μ_0 are vacuum permittivity and permeability, and ε and μ are the relative permittivity and permeability of the chiral molecule. c_0 is the speed of light in free-space, and κ , normalized by c_0 , is the dimensionless chiral parameter, which describes the chiroptical response of the chiral media. We note that the real and imaginary parts of the κ are related to the optical rotatory dispersion and the CD, respectively.

For a better demonstration of how the numerical calculation of weak total CD signals from a chiral molecule/nanostructure coupled system can be hampered by CD_{mesh} , we consider three representative values of the pure-real/imaginary chiral parameter κ of the molecule²⁴, 0.0001, 0.001, and 0.01, to consider the cases of weak, intermediate, and strong chiral responses, respectively. Here, the maximum discrete grid size is set at 40 nm for all FEM simulations. Figure 4(d,e) show FEM-calculated CD spectra considering the three pure-imaginary κ by adopting non-MSM and MSM. As shown in Fig. 4(e), the CD spectra by MSM exhibit identical line-shapes for the given values of κ . However, Fig. 4(d) clearly shows that FEM by non-MSM does not provide accurate CD values, as the CD spectra strongly differ from those by MSM and there is no consistency of spectral line-shape with varying κ . In particular, note that the discrepancies between the results obtained with MSM and non-MSM become more pronounced as κ decreases. The origin of the discrepancy is CD_{mesh} , the dotted-curve in Fig. 4(d), which is obtained by turning off the chiral parameter ($\kappa = 0$). CD_{mesh} is not negligible since its magnitude is comparable to those of the *pure* CDs obtained by applying MSM to the weak and intermediate cases ($\kappa = 0.001i$ and $0.0001i$). Similarly, in the case of the purely real-valued κ shown in Fig. 4(f,g), non-MSM does not provide reliable CD results while MSM generates consistently identical CD line-shapes. Again, the discrepancy between the results from MSM and non-MSM is more pronounced with smaller κ . Therefore, suppressing the numerical artifact is particularly important in the calculation of CDs from chiral molecules that exhibit weak chiral responses.

We further applied our MSM to the calculation of extremely weak CD signals. Figure 5 shows the CD signals of the chiral molecule/nanostructure coupled system with an even smaller κ . For both pure-imaginary (Fig. 5(a)) and pure-real (Fig. 5(b)) κ , MSM gives consistent CD spectra even at the low magnitude of 10^{-10} , far-lower than that of the CD_{mesh} . This suggests that our MSM enables numerical calculation of extremely weak CD signals, such as the calculation of CD from a system featuring dilute chiral molecule solutions.

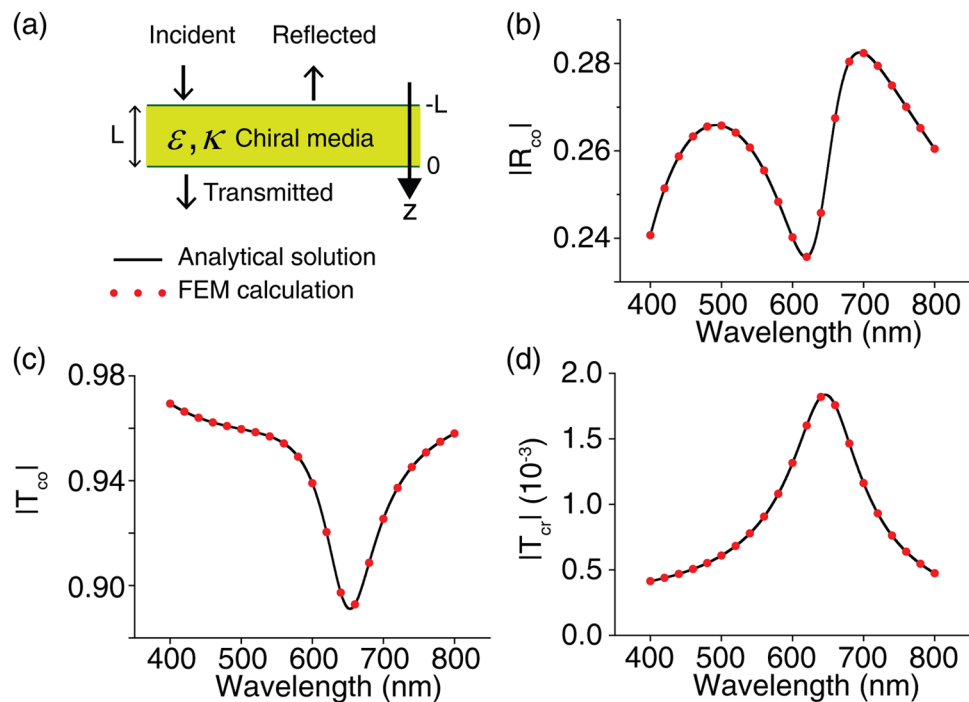


Figure 7. Validity of the numerical implementation of the chiral media in FEM. (a) A schematic of a free-standing chiral slab of thickness $L = 100$ nm. The frequency dependent dielectric constant and chiral parameter κ of the slab are given in Fig. 6(a,b), respectively. FEM-calculated (red dots) and analytically calculated (solid lines) spectra of (b) co-polarized reflection $|R_{co}|$, (c) co-polarized transmission $|T_{co}|$, and (d) cross-polarized transmission $|T_{cr}|$.

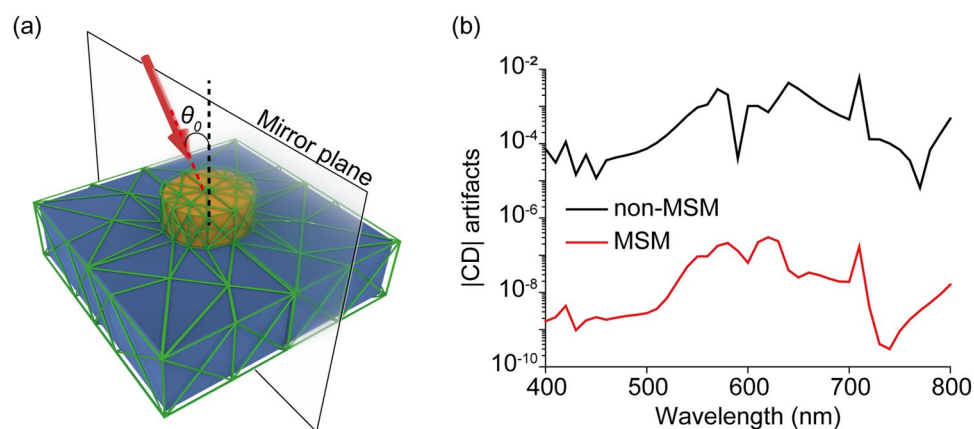


Figure 8. MSM for non-normal incidence case. (a) Non-normally incident light ($\theta_0 = 45^\circ$) to the periodic nanodisk array. (b) CD_{mesh} spectra of the nanodisk. CD should be zero since the nanodisk is achiral.

In principle, because CD_{mesh} is a numerical artifact related to the discretization of space, it can be suppressed by implementing smaller finite elements. This scheme is often used in the mesh convergence test which is an important procedure for the quantitative verification of numerical results²⁷. To check both the quantitative accuracy of results from MSM and for the possible suppression of CD_{mesh} in non-MSM, the chiral molecule/nanostructure coupled system is meshed with three different maximum-grid-sizes, d_{max} . Also, in order to take into account the more general chiral response of the molecule, we considered the complex dielectric constant and the chiral parameter as shown in Fig. 6(a,b), respectively: they are assumed to follow the Lorentz and Condon models. The resonance wavelength of the chiral molecules is intentionally set to be the same wavelength as LSPR to mimic the chiral response boost by the nanostructure. The FEM-calculated CD signals under the non-MSM and MSM schemes with three d_{max} values are shown in Fig. 6(c,d). It is clearly shown that decreasing d_{max} suppresses CD_{max} in the non-MSM case. However, unlike the MSM case in which the CD spectra are almost identical regardless of d_{max} , in the non-MSM case even reducing d_{max} from 40 nm to 20 nm does not yield fully-saturated results, since at 20 nm d_{max} an appreciable discrepancy still exists between the non-MSM and MSM CD spectra. Although

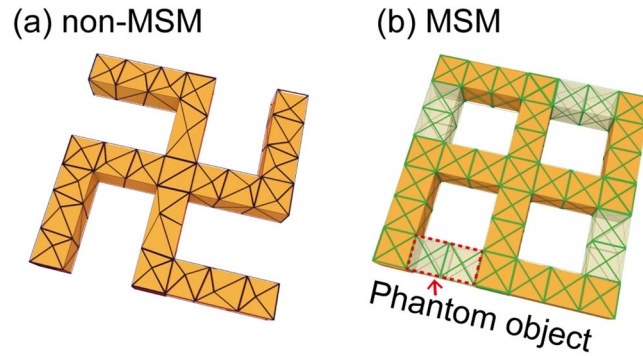


Figure 9. Implementation of MSM for chirally-arranged nanostructure. **(a)** An exemplary structure of a gammadion metamaterial. **(b)** MSM implemented by introducing phantom object.

further reductions in d_{\max} can be expected to produce more accurate results when using non-MSM, it should be noted that the size of the discrete grid is the main factor that trades off numerical accuracy for computational complexity. The results in Fig. 6 summarize that our MSM has a high tolerance for larger grid sizes, enabling computationally efficient and quantitatively accurate CD calculations.

Checking the numerical validity of the implementation of chiral media. The numerical validity of the implementation of chiral media is checked by comparing the numerically and analytically calculated chiral responses of the chiral molecule slab shown in Fig. 7(a). We used normally incident linearly polarized light, propagating along the z -direction. We compared three coefficients of the chiral slab: co-reflection R_{co} , co-transmission T_{co} , and cross-transmission T_{cr} , which can be calculated as²

$$R_{co} = \frac{(\eta_1\eta_2 - \eta_2\eta_3)\cos(k_2L) - i(\eta_1\eta_3 - \eta_2^2)\sin(k_2L)}{(\eta_1\eta_2 + \eta_2\eta_3)\cos(k_2L) - i(\eta_1\eta_3 + \eta_2^2)\sin(k_2L)}, \quad (3)$$

$$T_{co} = \frac{2\eta_2\eta_3 \cos(\kappa_r k_2L)}{(\eta_1\eta_2 + \eta_2\eta_3)\cos(k_2L) - i(\eta_1\eta_3 + \eta_2^2)\sin(k_2L)}, \quad (4)$$

$$T_{cr} = \frac{-2\eta_2\eta_3 \sin(\kappa_r k_2L)}{(\eta_1\eta_2 + \eta_2\eta_3)\cos(k_2L) - i(\eta_1\eta_3 + \eta_2^2)\sin(k_2L)}, \quad (5)$$

where k_2 is the wavenumber of light in the chiral slab, and L is the thickness of the slab. Note that the cross-reflection R_{cr} is zero for all values of κ . We assume that the chiral slab is freestanding, so that impedances of the incident region ($-L < z < 0$) η_1 and the transmitted region ($0 < z$) η_3 become the impedance of the vacuum: $\eta_1 = \eta_3 = \eta_0 = \sqrt{\mu_0/\epsilon_0}$. We also assumed that the slab possesses the exemplary dielectric constant and chiral parameter shown in Fig. 6(a,b), respectively. Results from the FEM calculation and analytic model are shown in Fig. 7(b-d). All the numerical results perfectly agree with the analytical theory, confirming that chiral media are well implemented by our FEM simulation.

Discussion

So far, we have considered only the case of normal incidence. We note that our mirror symmetric meshing (MSM) scheme can be extended to the case of non-normal incidence by taking the mirror plane to contain the light wavevector. For an exemplary demonstration, we studied the optical response of a periodic nanodisk array to an incoming light with incidence angle $\theta_0 = 45^\circ$ with respect to the vertical axis of the simulation domain, as shown in Fig. 8(a). Explicit calculation, with results in Fig. 8(b), shows that CD_{mesh} of non-MSM is about thousand-times larger than that of MSM with the mirror plane shown in Fig. 8(a).

We also note that our MSM scheme can be extended to the case of chiral structures made of non-chiral materials. In order to construct MSM for systems without mirror-symmetry, we introduce phantom objects to restore the mirror symmetry and create mirror-symmetric mesh without actually changing the real structure. Figure 9(a) presents an exemplary chiral gammadion structure. We change the gammadion into an achiral structure by minimally adding phantom object and create MSM and then remove the phantom part. The resulting mesh is given in Fig. 9(b) and explicit calculation shows significantly reduced CD_{mesh} .

In conclusion, we introduced a mirror symmetric mesh (MSM) scheme that can be applied to the finite element method (FEM) for numerical calculations of circular dichroism (CD). We demonstrated that unwanted numerical artifacts in CD, arising from improperly discretized problem spaces, can be strongly suppressed by adopting MSM. Our MSM scheme was tested through the calculation of CD from a chiral molecule/nanodisk coupled system, and we showed that MSM exhibits much faster numerical convergence and superior numerical reliability than the usual meshing scheme, enabling efficient and accurate CD calculations.

References

- Barron, L. D. *Molecular Light Scattering and Optical Activity*. 2nd edn (Cambridge University Press: Cambridge, 2004).
- Lindell, I. V. *Electromagnetic Waves in Chiral and Bi-Isotropic Media*. (Artech House, 1994).
- Lee, S., Yoo, S. & Park, Q. H. Microscopic Origin of Surface-Enhanced Circular Dichroism. *ACS Photonics* **4**, 2047–2052 (2017).
- Tang, Y. & Cohen, A. E. Optical chirality and its interaction with matter. *Phys. Rev. Lett.* **104**, 1–4 (2010).
- Tang, Y. & Cohen, A. E. Enhanced Enantioselectivity in Excitation of Chiral Molecules by Superchiral Light. *Science*. **332**, 333–336 (2011).
- García-Etxarri, A. & Dionne, J. A. Surface-enhanced circular dichroism spectroscopy mediated by nonchiral nanoantennas. *Phys. Rev. B - Condens. Matter Mater. Phys.* **87**, 1–5 (2013).
- Yoo, S., Cho, M. & Park, Q. H. Globally enhanced chiral field generation by negative-index metamaterials. *Phys. Rev. B - Condens. Matter Mater. Phys.* **89**, 1–5 (2014).
- Yoo, S. & Park, Q.-H. Enhancement of Chiroptical Signals by Circular Differential Mie Scattering of Nanoparticles. *Sci. Rep.* **5**, 14463 (2015).
- Hendry, E. *et al.* Ultrasensitive detection and characterization of biomolecules using superchiral fields. *Nat Nanotechnol* **5**, 783–787 (2010).
- Davis, T. J. & Hendry, E. Superchiral electromagnetic fields created by surface plasmons in nonchiral metallic nanostructures. *Phys. Rev. B - Condens. Matter Mater. Phys.* **87**, 1–5 (2013).
- Schäferling, M., Yin, X. & Giessen, H. Formation of chiral fields in a symmetric environment. *Opt. Express* **20**, 26326–26336 (2012).
- Nesterov, M. L., Yin, X., Schäferling, M., Giessen, H. & Weiss, T. The Role of Plasmon-Generated Near Fields for Enhanced Circular Dichroism Spectroscopy. *ACS Photonics* **3**, 578–583 (2016).
- Schäferling, M., Dregely, D., Hentschel, M. & Giessen, H. Tailoring enhanced optical chirality: Design principles for chiral plasmonic nanostructures. *Phys. Rev. X* **2**, 1–9 (2012).
- Maoz, B. M. *et al.* Amplification of chiroptical activity of chiral biomolecules by surface plasmons. *Nano Lett.* **13**, 1203–1209 (2013).
- Abdulrahman, N. A. *et al.* Induced chirality through electromagnetic coupling between chiral molecular layers and plasmonic nanostructures. *Nano Lett.* **12**, 977–983 (2012).
- Yoo, S. & Park, Q. H. Chiral Light-Matter Interaction in Optical Resonators. *Phys. Rev. Lett.* **114**, 1–5 (2015).
- Graf, P. *et al.* Silicification of peptide-coated silver nanoparticles-A biomimetic soft chemistry approach toward chiral hybrid core-shell materials. *ACS Nano* **5**, 820–833 (2011).
- Akyurtlu, A. & Werner, D. H. BI-FDTD: A novel finite-difference time-domain formulation for modeling wave propagation in bi-isotropic media. *IEEE Trans. Antennas Propag.* **52**, 416–425 (2004).
- Pereda, J. A., Grande, A., González, O. & Vegas, Á. FDTD modeling of chiral media by using the mobius transformation technique. *IEEE Antennas Wirel. Propag. Lett.* **5**, 327–330 (2006).
- Alkan, E., Demir, V., Elsherbeni, A. Z. & Arvas, E. Dual-grid finite-difference frequency-domain method for modeling chiral medium. *IEEE Trans. Antennas Propag.* **58**, 817–823 (2010).
- Klimov, V. V., Zabkov, I. V., Pavlov, A. A. & Guzatov, D. V. Eigen oscillations of a chiral sphere and their influence on radiation of chiral molecules. *Opt. Express* **22**, 18564–18578 (2014).
- Liu, Y., Gralak, B., McPhedran, R. C. & Guenneau, S. Finite frequency external cloaking with complementary bianisotropic media. *Opt. Express* **22**, 17387 (2014).
- www.comsol.com.
- Fasman, G. D., Fasman, E. B. E. *Circular Dichroism and the Conformational Analysis of Biomolecules*. (Plenum Press, New York, 1996).
- Govorov, A. O., Fan, Z., Hernandez, P., Slocik, J. M. & Naik, R. R. Theory of circular dichroism of nanomaterials comprising chiral molecules and nanocrystals: Plasmon enhancement, dipole interactions, and dielectric effects. *Nano Lett.* **10**, 1374–1382 (2010).
- Govorov, A. O. *et al.* Chiral nanoparticle assemblies: circular dichroism, plasmonic interactions, and exciton effects. *J. Mater. Chem.* **21**, 16806 (2011).
- Olek, C. Z. & Robert, L. T. *The Finite Element Method: Its Basis and Fundamentals*. 7th (Butterworth-Heinemann, 2013).

Acknowledgements

This work was supported by the Center for Advanced MetaMaterials (CAMM), funded by the Ministry of Science, ICT and Future Planning as Global Frontier Project (CAMM- 2014M3A6B3063710). J. H. Kang was supported by the Basic Science Research Program through the National Research Foundation of Korea (NRF) grant funded by the Korea government (MSIP) (NRF-2018R1C1B6009007). SeokJae Yoo was supported by Basic Science Research Program through the NRF funded by the Ministry of Education (2017R1A6A3A11034238).

Author Contributions

S.L. and Q.P. conceived the project. S.L. performed the numerical calculation, and S.L. and J.K prepared the figures. All authors discussed the results and contributed to writing the manuscript.

Additional Information

Competing Interests: The authors declare no competing interests.

Publisher's note: Springer Nature remains neutral with regard to jurisdictional claims in published maps and institutional affiliations.



Open Access This article is licensed under a Creative Commons Attribution 4.0 International License, which permits use, sharing, adaptation, distribution and reproduction in any medium or format, as long as you give appropriate credit to the original author(s) and the source, provide a link to the Creative Commons license, and indicate if changes were made. The images or other third party material in this article are included in the article's Creative Commons license, unless indicated otherwise in a credit line to the material. If material is not included in the article's Creative Commons license and your intended use is not permitted by statutory regulation or exceeds the permitted use, you will need to obtain permission directly from the copyright holder. To view a copy of this license, visit <http://creativecommons.org/licenses/by/4.0/>.

© The Author(s) 2018